ELECTROCHEMISTRY

Combining scaling relationships overcomes rate versus overpotential trade-offs in O_2 molecular electrocatalysis

Daniel J. Martin, Brandon Q. Mercado, James M. Mayer*

The development of advanced chemical-to-electrical energy conversions requires fast and efficient electrocatalysis of multielectron/multiproton reactions, such as the oxygen reduction reaction (ORR). Using molecular catalysts, correlations between the reaction rate and energy efficiency have recently been identified. Improved catalysis requires circumventing the rate versus overpotential trade-offs implied by such "scaling relationships." Described here is an ORR system—using a soluble iron porphyrin and weak acids—with the best reported combination of rate and efficiency for a soluble ORR catalyst. This advance is achieved not by "breaking" scaling relationships but rather by combining two of them. Key to this behavior is a polycationic ligand, which enhances anionic ligand binding and changes the catalyst $E_{1/2}$. These results show how combining scaling relationships is a powerful way toward improved electrocatalysis.

INTRODUCTION

Improving the rates and efficiencies of electrocatalytic reactions is critical to the development of chemical-to-electrical energy conversion technologies. The oxygen reduction reaction (ORR)—the combination of dioxygen (O_2), protons, and electrons to give water—is an important example common to fuel cells (*1*, *2*). Because current ORR technologies use platinum catalysts, current research seeks replacements sourced from earth-abundant materials (*3*). One approach to developing catalytic systems with high rates [turnover frequencies (TOFs)] and high efficiencies (low overpotentials, η) has been the development of scaling relationships. The properties of heterogeneous electrocatalysts can often be understood and even predicted using a single scaling descriptor, typically the energy of substrate binding to the catalyst surface (*4*). In contrast, soluble molecular electrocatalysts, which can be studied in more atomistic and mechanistic detail, follow multiple kinetic/thermodynamic scaling relationships (*5*). These describe how the maximum TOFs [$\log(TOF_{max})$] scale with the various terms contributing to the effective overpotential (η_{eff}) (*5*–*8*) (see the Supplementary Materials). To date, the reported $\log(TOF_{max})/\eta_{eff}$ relationships always describe a trade-off: Faster catalysis is only achieved at lower efficiencies (higher η_{eff}).

We report here an inverse scaling relationship, one that allows for faster rates at higher efficiencies, using a polycationic iron porphyrin catalyst with buffered weak acids in acetonitrile (MeCN) (Fig. 1A). With acetic acid/acetate buffer ($AcOH/AcO^-$), this system achieves a TOF_{max} of 170 s^{-1} at 0.54 V η_{eff}, which is ~10^4 faster than any previously reported molecular ORR catalyst at this η_{eff} (*2*, *9*). As described below, this unprecedented result is predictable by combining two kinetic/thermodynamic scaling relationships. The coupling of the two scaling relationships is a result of the electrostatic ligand design of **1** that enables cooperativity between the catalyst and buffer.

RESULTS

Iron αβαβ-*tetra*(*o*-*N*,*N*′,*N*″-trimethylanilinium)porphyrin (**1**) was prepared as reported (*10*) and was isolated and characterized as the di-aquo, penta-triflate salt of the αβαβ isomer by single-crystal x-ray diffraction (Fig. 1C). Cyclic voltammograms (CVs) of **1** in MeCN containing 0.1 M tetra-*n*-butylammonium tetrafluoroborate electrolyte ([*n*-Bu_4N][BF_4]) showed three reversible redox features ($Fe^{III/II}$, $Fe^{II/I}$, and $Fe^{I/0}$ (*10*). Solutions containing **1**, O_2, and buffered acid (1:1 [HA]/[A^-]) showed a large, irreversible current at the Fe^{III}/Fe^{II} reduction potential, indicative of catalysis (*5*, *7*, *11*). All CV experiments were buffered (1:1 acid-to-conjugate base) to define the ORR equilibrium potential and η_{eff}, which was calculated using Eq. 1 (*5*, *7*, *11*).

Measurements of the H_2O/H_2O_2 selectivity were performed using rotating ring disk electrochemistry (RRDE). In all cases, electrocatalysis was found to give <20% H_2O_2 (see the Supplementary Materials). This high selectivity for H_2O is similar to other iron porphyrin catalysts under comparable conditions (*5*, *7*, *11*). With $AcOH/AcO^-$ buffer, catalysis occurs at potentials below the equilibrium potential for O_2 to H_2O_2 and thus requires thermodynamic selectivity for H_2O [cf., (*9*)].

TOF_{max} values were determined from the catalytic CVs by foot-of-the-wave analysis (FOWA), Eq. 2 [Table 1; (*5*, *11*, *12*)]. This widely used approach normalizes the catalytic currents (i_c) to the noncatalytic peak current of the $Fe^{III/II}$ couple (i_p) at potentials (E) near the onset of the catalytic wave, where complications such as substrate depletion are minimized. Given the high selectivity for H_2O, n_{cat} was taken to be 4 (electrons per O_2 reduced), and the conservative σ = 1 value was used (see the Supplementary Materials). Measuring TOF_{max} values under different conditions showed that the catalytic rate law was first order in [**1**], P_{O2}, and [HA], similar to other Fe(por) catalysts (*5*, *7*, *11*). [HA] is the concentration of free acid after considering homoconjugation (see the Supplementary Materials). These results implicate a catalytic mechanism of (i) initial reduction of $[Fe^{III}(por)]^+$ to $Fe^{II}(por)$, (ii) pre-equilibrium O_2 binding to form the superoxide complex, $Fe^{III}(por)(O_2^{\bullet-})$, and (iii) rate-limiting proton transfer to form $[Fe^{III}(por)(O_2H^{\bullet})]^+$ (Fig. 1B). Experimental and computational studies of this mechanism are reported in (*5*, *11*, *12*).

$$\eta_{eff} = E^{o}_{ORR} - E_{1/2} - \frac{2.303RT}{n_{cat}F}\log\left(\frac{[H_2O]^2[A^-]^4}{P_{O_2}[HA]^4}\right) - (0.0592V)\,p\,K_a \quad (1)$$

$$\frac{i_c}{i_p} = \frac{2.24\,n_{cat}^{\sigma}\sqrt{\frac{RT}{Fv}TOF_{max}}}{1+\exp\left[\frac{F}{RT}(E-E_{1/2})\right]} \quad (2)$$

Yale University, Department of Chemistry, New Haven, CT, USA.
*Corresponding author. Email: james.mayer@yale.edu

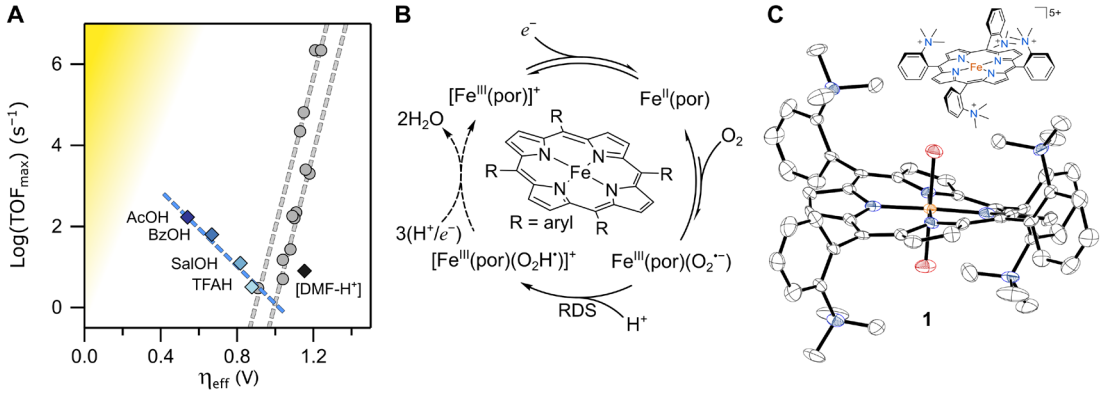

Fig. 1. Catalytic system efficiencies, reaction mechanism, and structure of catalyst 1. (**A**) Plot of log(TOF$_{max}$)/η_{eff} values and fits (dashed lines) for **1** (diamonds; data and conditions in Table 1) and for previously reported iron porphyrin [Fe(por)] catalysts (circles; 0.1 M [DMF-H$^+$] in DMF or MeCN) (*5*). The uncertainties are smaller than the data points. The yellow shading indicates an aspirational region. (**B**) Fe(por) catalyzed O_2 reduction mechanism, as described in the main text (*11*). (**C**) Drawings of **1** and of the cation in the solid-state x-ray crystal structure, [**1**•2H$_2$O]OTf$_5$ (Fe, orange; N, blue; C, white; O, red; H atoms omitted for clarity; thermal ellipsoids at 50% probability).

Table 1. Properties of catalytic systems with 1 and different buffers. Experimental conditions: 0.1 mM **1**, 0.1 M buffer (1:1 HA/A or HB$^+$/B), 0.1 M [*n*-Bu$_4$N][BF$_4$] in MeCN (~15 mM H_2O), 1 atm O_2. [DMF-H$^+$], *N*,*N*′-dimethylformamidium triflate; TFAH, trifluoroacetic acid; [Lut-H$^+$], lutidinium tetrafluoroborate; SalOH, salicylic acid; BzOH, benzoic acid; AcOH, acetic acid.

Buffer	pK_a*	$E_{1/2}$ (V)†	η_{eff} (V)‡	TOF$_{max}$ (s^{-1})§	log(TOF$_{max}$)
None	–	−0.295	–	–	–
[DMF-H$^+$]/DMF	6.1	−0.25*	1.16	8.5	0.91
TFAH/TFA$^-$	12.6	−0.349	0.88	3.2	0.51
[Lut-H$^+$]/Lut	14.1	−0.23*	0.68	0.07	−1.17
SalOH/SalO$^-$	16.7	−0.536	0.82	12	1.08
BzOH/BzO$^-$	21.5	−0.653	0.67	63	1.80
AcOH/AcO$^-$	23.5	−0.651	0.54	170	2.23

*See the Supplementary Materials. †$E_{1/2}$(Fe$^{III/II}$) reduction potential (versus ferrocenium/ferrocene, under Ar, with 100 mM buffer). ‡From Eq. 2; ±0.02 V. §From FOWA.

ORR catalysis was studied in MeCN using **1** and a series of buffers. Using *N*,*N*′-dimethylformamidium triflate ([DMF-H$^+$]OTf; pK_a =6.1, where K_a is the acid dissociation constant), TOF$_{max}$ = 8.5 s^{-1} and η_{eff} = 1.16 V (Table 1). Within the log(TOF$_{max}$)/η_{eff} space, this [η_{eff}, log(TOF$_{max}$)] data point roughly fits the scaling relationships previously reported for Fe(por) electrocatalysts under similar conditions (Fig. 1A, black diamond) (*5*). In contrast, using acetic acid (AcOH, pK_a = 23.5) gave markedly improved catalysis: a faster TOF$_{max}$ (170 s^{-1}) at less than half the η_{eff} (0.54 V). This result contradicts previously derived log(TOF$_{max}$)/η_{eff} relationships, which always predict that a lower overpotential will give a slower rate, as seen for iron tetra-arylporphyrins (see the Supplementary Materials) (*7*). Catalysis with **1** and trifluoroacetic acid (TFAH), salicylic acid (SalOH), or benzoic acid (BzOH) similarly show improvements in both TOF$_{max}$ and η_{eff} versus the [DMF-H$^+$] point (Fig. 1, blue diamonds, and Table 1). Together, the carboxylic acid [η_{eff}, log(TOF$_{max}$)] points define an unexpected inverse log(TOF$_{max}$)/η_{eff} relationship (Fig. 1A, blue dashed line), a previously unrealized goal in molecular electrocatalysis (*5*, *13*, *14*). The following sections describe a model that explains this inverse relationship as the sum of two known kinetic/thermodynamic scaling relationships (*7*).

DISCUSSION

Catalyst **1** is unique among the Fe(por) series because changing the buffer notably affects two properties of the catalytic system: the acid pK_a and also the catalyst $E_{1/2}$, due to carboxylate binding. Since both pK_a and $E_{1/2}$ each modulate the TOF$_{max}$ and η_{eff} in different ways [see the Supplementary Materials and (*5*, *7*) for further discussion], a single scaling relationship is not adequate for predicting the composite changes in log(TOF$_{max}$)/η_{eff}. Instead, the scaling relationships—which only establish directionality within the log(TOF$_{max}$)/η_{eff} space—must be recast as vectors. Vectors have directionality and length and are additive.

The Nernst equation for this ORR reaction (Eq. 1) shows that a one-unit increase in acid pK_a decreases η_{eff} by 0.059 V: $\Delta\eta_{eff}$ = −(0.059 V)ΔpK_a (*15*, *16*). In iron porphyrin ORR catalysis, protonation is the rate-determining step, and the TOF$_{max}$ varies with pK_a according to the Brønsted equation: Δlog(TOF$_{max}$) = −α(ΔpK_a), where $\alpha \approx 0.3$ (*5*, *7*, *11*). For the range of carboxylate buffers used here, TFAH/TFA$^-$ to AcOH/AcO$^-$, the change in pK_a is 10.9. Therefore, with α = 0.3 and holding all other properties constant, the changes in η_{eff} and log(TOF$_{max}$) associated with the 10.9 pK_a shift can be

described as the vector $\vec{v}_{pK_a}$ in the [η_{eff}, log(TOF$_{max}$)] space (Eq. 3, dec stands for decade in TOF$_{max}$; Fig. 3).

$$\vec{v}_{pK_a} = \langle \Delta\eta_{eff}, \Delta\log(TOF_{max}) \rangle = \langle -0.059(\Delta pK_a), -\alpha(\Delta pK_a) \rangle = \langle -0.64\ V, -3.3\ dec \rangle \quad (3)$$

In addition to acid pK_a, the buffer identity also affects the $E_{1/2}$. When buffered carboxylic acids are titrated into solutions of **1**, the catalyst $E_{1/2}$ shifts negatively, by as much as 350 mV (Fig. 2A). This shift results from the conjugate base of the buffer (e.g., acetate) binding more strongly to the Fe^{III} versus the Fe^{II} form of **1**. This behavior was documented and explained many years ago for chloride binding to iron tetraphenylporphyrin (*17*). At 0.1 M carboxylate buffer, the $E_{1/2}$ values vary linearly with acid pK_a (−28 ± 1 mV/pK_a; Fig. 2B). In contrast, buffers with cationic acids and neutral conjugate bases ([DMF-H$^+$]/DMF and [Lut-H$^+$]/Lut) give only small shifts in $E_{1/2}$ (<50 mV; Fig. 2B). This unique distinction is due to the highly cationic nature of **1**, which enhances binding of anionic conjugate bases but not neutral ones (see the Supplementary Materials). Further supporting the importance of the cationic ligand, no notable change in catalyst $E_{1/2}$ was reported when iron tetraphenylporphyrin—an analog without the cationic trimethylanilinium groups—was combined with similar buffers under similar conditions (*7*).

Changes in $E_{1/2}$ also affect η_{eff}: $\Delta\eta_{eff} = -\Delta E_{1/2}$ (Eq. 2) (*5*, *7*, *18*). For the Fe(por) series, log(TOF$_{max}$) has empirically been shown to change according to log(TOF$_{max}$) = −18.5 decade/$E_{1/2}$(V) (see the Supplementary Materials for further discussion) (*7*). Conceptually, this is because catalysts with more negative $E_{1/2}$s (and thus higher η_{eff}s) bind O_2 more strongly and form more basic superoxide complexes, both of which lead to higher TOF$_{max}$ (*5*). As above, a vector $\vec{v}_{E_{1/2}}$ can be used to represent the log(TOF$_{max}$)/$E_{1/2}$ scaling relation and the 0.302 V change in $E_{1/2}$ upon replacing TFAH/TFA$^-$ with AcOH/AcO$^-$ (Eq. 4 and Fig. 3)

$$\vec{v}_{E_{1/2}} = \langle \Delta\eta_{eff}, \Delta\log(TOF_{max}) \rangle = \langle -\Delta E_{1/2}, -18.5(\Delta E_{1/2}) \rangle = \langle 0.30\ V, 5.6\ dec \rangle \quad (4)$$

Because the buffer affects both the acid pK_a and catalyst $E_{1/2}$, both $\vec{v}_{pK_a}$ and $\vec{v}_{E_{1/2}}$ are needed to describe the changes in η_{eff} and log(TOF$_{max}$). The effects of these changes are additive, described by the vector sum: $\vec{v}_{sum} = \vec{v}_{pK_a} + \vec{v}_{E_{1/2}}$ (Eq 5 and Fig. 3). While neither $\vec{v}_{pK_a}$ nor $\vec{v}_{E_{1/2}}$ alone fits the observed changes in log(TOF$_{max}$)/η_{eff}, $\vec{v}_{sum}$ predicts both the directionality and distance from the experimental TFAH coordinate to the AcOH coordinate—within a factor of 3 in TOF$_{max}$.

$$\vec{v}_{sum} = \vec{v}_{pK_a} + \vec{v}_{E_{1/2}} = \langle -0.34\ V, 2.3\ dec \rangle \quad (5)$$

Qualitatively, using a less acidic buffer improves the overall catalysis because of two factors. The change in $E_{1/2}$ causes a large gain in TOF$_{max}$ at relatively little cost to η_{eff} (a steep scaling slope). In contrast, the concomitant changes in pK_a decrease η_{eff} substantially with only small losses in TOF$_{max}$ (a shallow slope). The combination is a faster TOF$_{max}$ at lower η_{eff}.

While $\vec{v}_{sum}$ is required to analyze the carboxylate buffer data, only $\vec{v}_{pK_a}$ is needed to predict the change in log(TOF$_{max}$)/η_{eff} for the cationic buffers (e.g., [DMF-H$^+$]/DMF and [Lut-H$^+$]/Lut) (Fig. 3B). This is because the change in cationic buffers affects primarily the pK_a, with little effect on the $E_{1/2}$. The lack of change in $E_{1/2}$ highlights the key role of the cationic macrocycle, which enhances anion binding but not binding of a neutral ligand. Unlike CO_2 electroreduction by catalyst **1** (*10*), the remarkable log(TOF$_{max}$)/η_{eff} data reported here are not just a feature of the catalyst but rather the combination of the catalyst and buffer.

The summative or "tandem" scaling relationship approach developed here is unexpectedly accurate given that the contributing scaling relationships were obtained for a somewhat different set of catalysts, iron porphyrins with different meso-aryl substituents. Yet,

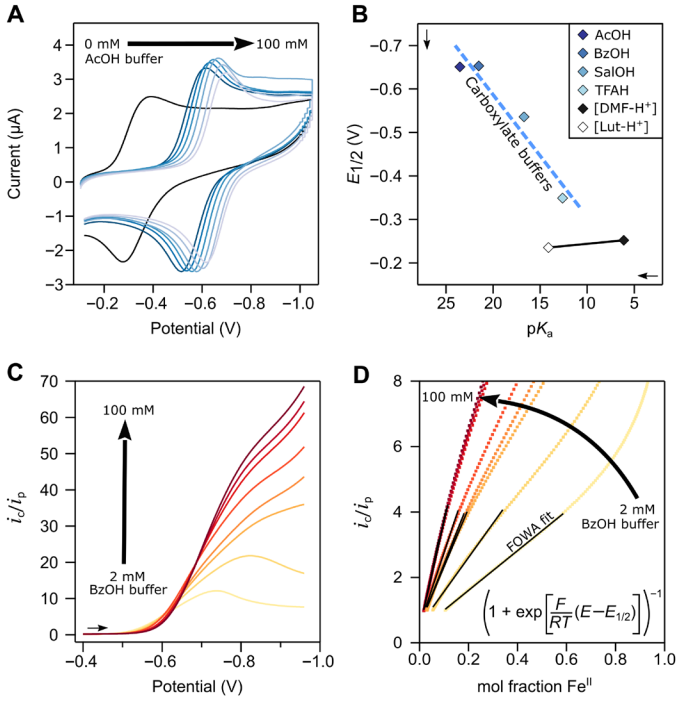

Fig. 2. Electrochemical studies of 1 under noncatalytic and catalytic conditions. (**A**) CVs of **1** showing the shift of $E_{1/2}$ with increasing concentrations of 1:1 AcOH/AcO$^-$ buffer. (**B**) Plot of $E_{1/2}$ versus the acid pK_a at 0.1 M buffer. (**C**) Linear sweep voltammograms under catalytic conditions with different BzOH buffer concentrations. (**D**) FOWA for voltammograms in (C), with fits between i_c/i_p = 1 to 4.

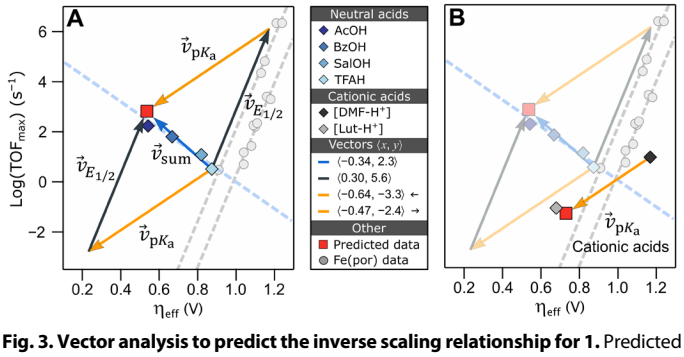

Fig. 3. Vector analysis to predict the inverse scaling relationship for 1. Predicted coordinates using the vectors are shown as red squares. (**A**) Plot of log(TOF$_{max}$) versus η_{eff} for catalytic systems of **1** and varying carboxylic acid buffers (data points match those in Fig. 1). Superimposed vectors (gold, black, and blue) show predicted changes caused by pK_a, $E_{1/2}$, and summative effects, respectively. (**B**) Buffers with cationic acids follow only the pK_a vector (gold). Prior Fe(por) data and $E_{1/2}$ scaling relationships (*7*) are included for reference (gray). Uncertainties are smaller than the data points.

these scaling relationships quantitatively hold for the different axial ligands in the **1** + buffer systems examined here. Paradoxically, the tandem approach circumvents the limitations implied by prior molecular scaling relationships—that there is always a trade-off between TOF_{max} and η_{eff}—because of the robustness and generality of the same "limiting" relationships.

Here, we show that kinetic/thermodynamic scaling relationships for molecular electrocatalysts can be additive and that this tandem scaling approach is a powerful and predictive way to improve multistep electrocatalytic processes. Specifically, summing multiple known scaling relationships predicted an unprecedented, inverse $\log(TOF)/\eta_{eff}$ relationship that allowed for simultaneous improvement in both catalysis rates and efficiencies. This approach has yielded the best reported combination of TOF and η_{eff} for a soluble ORR catalyst.

The ability to combine scaling relationships should be applicable beyond this case study. Optimization by this method, and perhaps even inverse scaling, only requires that the catalytic reaction have at least two properties that affect the TOF_{max} and η_{eff} in different ways (different slopes). Most molecular electrocatalysis meets this two-descriptor requirement because their mechanisms have pre-equilibrium and rate-limiting steps with different stoichiometries and/or different relationships between the k, K_{eq}, and the $\Delta G°$ for each step. ORR catalysis by **1** is a special case of the two-descriptor requirement because a single change to the system—changing the buffer—affects both the catalyst $E_{1/2}$ and the acid pK_a, each of which independently affects the pre-equilibrium and rate-determining steps. Ongoing work in our lab is extending this tandem scaling approach to simultaneous but independent changes in $E_{1/2}$ and pK_a, by changing both the catalyst and the buffer. A similar approach may also be applicable to heterogeneous electrocatalysis, since there is increasing recognition that those mechanisms may also have pre-equilibria and kinetic steps with different properties (*19*). Therefore, this method of combining scaling relationships may have ramifications for the development of both homogeneous and heterogeneous electrocatalysis of energy-important processes.

MATERIALS AND METHODS

Instrumentation

High-resolution mass spectrometry was performed using a Waters Xevo G2-XS QTof mass spectrometer. Ultraviolet-visible (UV-vis) optical spectra were recorded on an Agilent 8452 diode-array spectrometer and were collected using a 1-cm path length cuvette. Infrared (IR) spectrum was recorded on a Bruker Alpha Fourier transform infrared spectrophotometer equipped with an attenuated total reflectance (ATR) attachment. The electrochemical setup is described below. Information about the x-ray diffractometer is described below.

Materials

2-Nitrobenzaldehyde (Sigma-Aldrich, >95%), tin(II) chloride dihydrate (Sigma-Aldrich, >99%), aqueous hydrochloric acid [Macron, 36 to 38 weight % (wt %)], iron (II) bromide (Sigma-Aldrich, >98%), 2,6-lutidine (Sigma-Aldrich, ReagentPlus, >98%), formaldehyde (Sigma-Aldrich, 37 wt %, containing 10 to 15% methanol as stabilizer), sodium cyanoborohydride (Acros, >98%), methyltrifluoromethylsulfonate (MeOTf; Sigma-Aldrich, >98%), trifluoromethylsulfonic acid (Acros, 99%), neutral aluminum oxide (Sigma-Aldrich, >99%), silica (Sigma-Aldrich, >99%), sodium chloride (Sigma-Aldrich, >99%), sodium bicarbonate (Sigma-Aldrich, >99%), ammonium hydroxide solution (Sigma-Aldrich, 25 wt %), AcOH (Sigma-Aldrich, >99.9%), BzOH (Sigma-Aldrich, >99.5%), SalOH (Sigma-Aldrich, >99%), TFA (Sigma-Aldrich, ReagentPlus, >99%), tetra-*n*-butylammonium acetate (Sigma-Aldrich, 97%), tetra-*n*-butylammonium benzoate (Sigma-Aldrich, >99%), tetra-*n*-butylammonium salicylate [Tokyo Chemical Industry (TCI), 98%], and sodium trifluoroacetate (Sigma-Aldrich, 98%) were all used as received. All of the solid chemicals were stored in a N_2 glovebox when not in use.

Tetrahydrofuran, *N*,*N*′-dimethylformamide (DMF), MeCN, and diethyl ether were all degassed with argon and dried using a Pure Process Technology solvent system before use. Tetra-*n*-butylammonium tetrafluoroborate (Acros, >98%) was stored in a desiccator containing Drierite (calcium sulfate). Bis(cyclopentadienyl)iron(II) (ferrocene or Fc; Sigma-Aldrich, 95%) was recrystallized two times from hexanes before being dried in a N_2 glovebox. Pyrrole (Acros, 99%) was freshly distilled immediately before each use. The Pur-A-Lyzer Mega Dialysis Kit [Sigma-Aldrich, 1 kDa molecular weight cut-off (MWCO)] was soaked in Milli-Q water for 1 hour before dialysis of **1**. Dioxygen (Airgas, Ultra High Purity) and argon (Airgas, Ultra High Purity) were used as received. *N*,*N*′-dimethylformamidium triflate ([DMF-H]OTf) and 2,6-lutidinium triflate ([Lut-H]OTf) were synthesized using previously reported methods (*20*, *21*).

Synthesis of iron αβαβ-*tetra*(*o*-*N*,*N*′,*N*″-trimethylanilinium) porphyrin (1)

The synthesis of the known iron(III) α,β,α,β-5,10,15,20-tetra(ortho-*N*,*N*′,*N*″-trimethylanilinium)-porphyrin penta(trifluoromethanesulfonate), **1**, was slightly adapted from literature preparation (*10*). The α,β,α,β-5,10,15,20-tetra(ortho-aminophenyl)porphyrin atropoisomer was isolated chromatographically using the conditions described in (*10*). Later in the synthesis, during the final methylation reaction of iron(III) α,β,α,β-5,10,15,20-tetra(ortho-*N*,*N*′-dimethylaminophenyl)porphyrin chloride [chart S1, product **4**, from reference (*10*)] to the fully quaternized product, 300-equivalent MeOTf were used in place of the reported 100 equivalents. Full quaternization was supported by the high-resolution mass spectrum (HRMS) (which did not reveal any partially quaternized products) and by cyclic voltammetry (see the Supplementary Materials). The product, which was collected in identical yields to the initial report, was purified by dialysis against Milli-Q water (10 ml of sample inside dialyzing bag, 250 ml of surrounding water replaced every 90 min for a total of 12 hours). The product was then recrystallized via slow vapor diffusion of diethyl ether into MeCN containing the iron porphyrin. This recrystallization method yielded crystals suitable for x-ray diffraction (see the Supplementary Materials). HRMS [electron spray ionization (ESI)/quadrupole orthogonal acceleration–time-of-flight) mass/charge ratio (*m*/*z*): $([M]^{5+} + 4OTf^-)$ calculated (calcd) for $C_{56}H_{60}FeN_8(CF_3SO_3)_4$ 1496.2373; found 1496.2493. $([M]^{5+} + 3OTf^-)$ calcd for $C_{56}H_{60}FeN_8(CF_3SO_3)_3$ 673.6426; found 673.6395. UV-vis and IR spectra also agree with what was reported in reference (*10*), see the Supplementary Materials.

Electrochemical methods

CV was performed on a CH Instruments model 650D potentiostat. RRDE was conducted using a BASi Epsilon potentiostat and a Pine Instruments rotator (see the Supplementary Materials for further details). CVs used a 3-mm glassy carbon working electrode, a platinum wire counter electrode, and a Ag wire pseudoreference. The

Ag wire pseudoreference was prepared using the method reported by Dempsey *et al.* (*22*), where a silver wire was sanded and fit snuggly into a capillary containing MeCN and 0.1 M [*n*-Bu_4N][BF_4]. The solution inside the capillary was separated from bulk solutions using a Vycor tip that had been mechanically sealed to the capillary using heat shrink tubing. The capillary was stored in a solution containing 0.1 M [*n*-Bu_4N][BF_4] in-between experiments. For analysis, each voltammogram was internally referenced to ferrocene. The glassy carbon working electrodes were polished after every voltammogram by vigorously polishing on a Buehler felt pad to a mirror-like finish using an alumina slurry (wetted 0.05-μm alumina powder). After polishing, the electrode was rinsed with water and MeCN. Internal resistance (iR) compensation was performed before each voltammogram using the CH Instruments integrated software. The typical resistance value was <60 ohm. Considering the typical amount of current passed during catalysis (~200 μA), the iR compensation shifted the potential response of <10 mV for most experiments.

All of the buffered electrochemical experiments were performed with a one-to-one buffer of acid and conjugate base. Throughout, we identify the initial buffer concentrations rather than expressly list the acid and conjugate base concentrations. For example, a "10 mM AcOH buffer" means that the solution was prepared to initially contain 10 mM AcOH and 10 mM AcO^-. These values do not necessarily reflect the concentrations of nonhomoconjugated acid and base (see the Supplementary Materials).

Electrocatalytic, aerobic measurements were performed after sparging the buffered solution and headspace with O_2. The sparging was performed with pure O_2 at 1 atm unless otherwise noted. To minimize solvent evaporation and accompanying temperature changes, the O_2 was first sparged through an initial bubbler containing pure MeCN. Between each catalytic voltammogram, the working electrode was vigorously polished (see above). To ensure reproducibility, each catalytic voltammogram was also performed in duplicate, and the rates were averaged (see the Supplementary Materials). Unless otherwise specified, every voltammogram reported was collected at 0.1 V/s in a MeCN solution containing 0.1 mM **1** and 0.1 M [*n*-Bu_4N][BF_4].

Single-crystal x-ray diffraction

Crystals of [Fe-*o*-TMA]OTf_5•$2H_2O$ (identification code 007b-17062) were grown by slow vapor diffusion of diethyl ether into MeCN on the benchtop. Two water molecules were identified as axial ligands in the solid-state structure. Low-temperature diffraction data (ω-scans) were collected on a Rigaku MicroMax-007HF diffractometer coupled to a Saturn994+ charge-coupled device detector with Cu Kα (λ = 1.54178 Å) for the structure of [Fe-*o*-TMA]OTf_5•$2H_2O$. The diffraction images were processed and scaled using Rigaku Oxford Diffraction software. The structure was solved with SHELXT and was refined against F^2 on all data by full-matrix least squares with SHELXL (*23*). The data were refined as an inversion twin. The fractional volume contributions of the second twin component were refined to a value of 0.432(18). All nonhydrogen atoms were refined anisotropically. Hydrogen atoms were included in the model at geometrically calculated positions and refined using a riding model. The isotropic displacement parameters of all hydrogen atoms were fixed 1.2 times the *U* value of the atoms to which they are linked (1.5 times for methyl groups). The Fe-O distance was measured to be 2.101(8) Å, which suggested the assignment as water.

The asymmetric unit of the crystallographic model contains 0.25 of the formula unit $C_{56}H_{64}FeN_8O_2$•$5(CF_3O_3S)$. The iron resides on the crystallographic $\bar{4}$ rotation axis at (0, ½, ¼). The asymmetric unit also contains a quarter of the porphyrin and 1.25 triflates. One triflate site is on a general position (*x*,*y*,*z*), and the other site is near the crystallographic $\bar{4}$ rotation axis (½, ½, ½).

The triflate on the general position is disordered over two sites. The thermal ellipsoids for the triflate atoms were restrained to behave as rigid bodies. The site occupancies were fixed at 0.50, and all chemically equivalent 1,2 and 1,3 distances were restrained to be similar. The other triflate was disordered with respect to the $\bar{4}$ rotation axis. This modeled triflate was placed as a constrained, rigid group based on the difference map (see the Supplementary Materials). The special position constraints were suppressed, and the model occupancy was fixed at 0.25. The program SQUEEZE (*24*) was used to compensate for the contribution of disordered solvents contained in voids within the crystal lattice from the diffraction intensities. This procedure was applied to the data file, and the submitted model is based on the solvent removed data. On the basis of the total electron density found in the voids (181 e/$Å^3$), it is possible that some combination of crystallization solvents is present in the unit cell. See "_platon_squeeze_ details" in this .cif for more information.

The full details of the x-ray structure determination (CIF) can be found in the Cambridge Crystallographic Data Center (CCDC), number 1947226 ([Fe-*o*-TMA]OTf_5•$2H_2O$). These data can be obtained free of charge from the CCDC via www.ccdc.cam.ac.uk/data_request/cif.

SUPPLEMENTARY MATERIALS

Supplementary material for this article is available at http://advances.sciencemag.org/cgi/content/full/6/11/eaaz3318/DC1

REFERENCES AND NOTES

1. E. I. Solomon, S. S. Stahl, Introduction: Oxygen reduction and activation in catalysis. *Chem. Rev.* **118**, 2299–2301 (2018).
2. M. L. Pegis, C. F. Wise, D. J. Martin, J. M. Mayer, Oxygen reduction by homogeneous molecular catalysts and electrocatalysts. *Chem. Rev.* **118**, 2340–2391 (2018).
3. A. A. Gewirth, J. A. Varnell, A. M. DiAscro, Nonprecious metal catalysts for oxygen reduction in heterogeneous aqueous systems. *Chem. Rev.* **118**, 2313–2339 (2018).
4. A. Kulkarni, S. Siahrostami, A. Patel, J. K. Nørskov, Understanding catalytic activity trends in the oxygen reduction reaction. *Chem. Rev.* **118**, 2302–2312 (2018).
5. M. L. Pegis, B. A. McKeown, N. Kumar, K. Lang, D. J. Wasylenko, X. P. Zhang, S. Raugei, J. M. Mayer, Homogenous electrocatalytic oxygen reduction rates correlate with reaction overpotential in acidic organic solutions. *ACS Cent. Sci.* **2**, 850–856 (2016).
6. C. M. Klug, A. J. P. Cardenas, R. M. Bullock, M. O'Hagan, E. S. Wiedner, Reversing the tradeoff between rate and overpotential in molecular electrocatalysts for H_2 production. *ACS Catal.* **8**, 3286–3296 (2018).
7. M. L. Pegis, C. F. Wise, B. Koronkiewicz, J. M. Mayer, Identifying and breaking scaling relations in molecular catalysis of electrochemical reactions. *J. Am. Chem. Soc.* **139**, 11000–11003 (2017).
8. Y.-H. Wang, M. L. Pegis, J. M. Mayer, S. S. Stahl, Molecular cobalt catalysts for O_2 reduction: Low-overpotential production of H_2O_2 and comparison with iron-based catalysts. *J. Am. Chem. Soc.* **139**, 16458–16461 (2017).
9. Y.-H. Wang, P. E. Schneider, Z. K. Goldsmith, B. Mondal, S. Hammes-Schiffer, S. S. Stahl, Brønsted acid scaling relationships enable control over product selectivity from O_2 reduction with a mononuclear cobalt porphyrin catalyst. *ACS Cent. Sci.* **5**, 1024–1034 (2019).
10. I. Azcarate, C. Costentin, M. Robert, J.-M. Savéant, Through-space charge interaction substituent effects in molecular catalysis leading to the design of the most efficient catalyst of CO_2-to-CO electrochemical conversion. *J. Am. Chem. Soc.* **138**, 16639–16644 (2016).
11. M. L. Pegis, D. J. Martin, C. F. Wise, A. C. Brezny, S. I. Johnson, L. E. Johnson, N. Kumar, S. Raugei, J. M. Mayer, Mechanism of catalytic O_2 reduction by iron tetraphenylporphyrin. *J. Am. Chem. Soc.* **141**, 8315–8326 (2019).
12. C. Costentin, G. Passard, J.-M. Savéant, Benchmarking of homogeneous electrocatalysts: Overpotential, turnover frequency, limiting turnover number. *J. Am. Chem. Soc.* **137**, 5461–5467 (2015).
13. V. Artero, J.-M. Savéant, Toward the rational benchmarking of homogeneous H_2-evolving catalysts. *Energ. Environ. Sci.* **7**, 3808–3814 (2014).
14. H. Liu, L. Wei, F. Liu, Z. Pei, J. Shi, Z. J. Wang, D. He, Y. Chen, Homogeneous, heterogeneous, and biological catalysts for electrochemical N_2 reduction toward NH_3 under ambient conditions. *ACS Catal.* **9**, 5245–5267 (2019).
15. A. M. Appel, M. L. Helm, Determining the overpotential for a molecular electrocatalyst. *ACS Catal.* **4**, 630–633 (2014).
16. G. Passard, D. K. Dogutan, M. Qiu, C. Costentin, D. G. Nocera, Oxygen reduction reaction promoted by manganese porphyrins. *ACS Catal.* **8**, 8671–8679 (2018).
17. D. Lexa, P. Rentien, J. M. Savéant, F. Xu, Methods for investigating the mechanistic and kinetic role of ligand exchange reactions in coordination electrochemistry. *J. Electroanal. Chem. Interfacial Electrochem.* **191**, 253–279 (1985).
18. G. Passard, A. M. Ullman, C. N. Brodsky, D. G. Nocera, Oxygen reduction catalysis at a dicobalt center: The relationship of faradaic efficiency to overpotential. *J. Am. Chem. Soc.* **138**, 2925–2928 (2016).
19. L. D. Chen, M. Bajdich, J. M. P. Martirez, C. M. Krauter, J. A. Gauthier, E. A. Carter, A. C. Luntz, K. Chan, J. K. Nørskov, Understanding the apparent fractional charge of protons in the aqueous electrochemical double layer. *Nat. Commun.* **9**, 3202 (2018).
20. B. D. McCarthy, J. L. Dempsey, Decoding proton-coupled electron transfer with potential–pK_a diagrams. *Inorg. Chem.* **56**, 1225–1231 (2017).
21. I. Favier, E. Duñach, New protic salts of aprotic polar solvents. *Tetrahedron Lett.* **45**, 3393–3395 (2004).
22. N. Elgrishi, K. J. Rountree, B. D. McCarthy, E. S. Rountree, T. T. Eisenhart, J. L. Dempsey, A practical beginner's guide to cyclic voltammetry. *J. Chem. Educ.* **95**, 197–206 (2017).
23. G. M. Sheldrick, A short history of *SHELX*. *Acta Cryst.* **64**, 112–122 (2008).
24. A. L. Spek, *PLATON SQUEEZE*: A tool for the calculation of the disordered solvent contribution to the calculated structure factors. *Acta Cryst.* **71**, 9–18 (2015).
25. M. Fang, M. H. Engelhard, Z. Zhu, M. L. Helm, J. A. S. Roberts, Electrodeposition from acidic solutions of nickel Bis(benzenedithiolate) produces a hydrogen-evolving Ni–S film on glassy carbon. *ACS Catal.* **4**, 90–98 (2014).
26. V. Artero, M. Fontecave, Solar fuels generation and molecular systems: Is it homogeneous or heterogeneous catalysis? *Chem. Soc. Rev.* **42**, 2338–2356 (2013).
27. F. A. Walker, U. Simonis, in *Encyclopedia of Inorganic Chemistry* (John Wiley & Sons Ltd., 2006).
28. J. A. S. Roberts, R. M. Bullock, Direct determination of equilibrium potentials for hydrogen oxidation/production by open circuit potential measurements in acetonitrile. *Inorg. Chem.* **52**, 3823–3835 (2013).
29. V. Fourmond, P.-A. Jacques, M. Fontecave, V. Artero, H_2 evolution and molecular electrocatalysts: Determination of overpotentials and effect of homoconjugation. *Inorg. Chem.* **49**, 10338–10347 (2010).
30. B. D. McCarthy, D. J. Martin, E. S. Rountree, A. C. Ullman, J. L. Dempsey, Electrochemical reduction of brønsted acids by glassy carbon in acetonitrile-implications for electrocatalytic hydrogen evolution. *Inorg. Chem.* **53**, 8350–8361 (2014).
31. M. L. Helm, M. P. Stewart, R. M. Bullock, M. R. DuBois, D. L. DuBois, A synthetic nickel electrocatalyst with a turnover frequency above 100,000 s^{-1} for H_2 production. *Science* **333**, 863–866 (2011).
32. M. P. Stewart, M.-H. Ho, S. Wiese, M. L. Lindstrom, C. E. Thogerson, S. Raugei, R. M. Bullock, M. L. Helm, High catalytic rates for hydrogen production using nickel electrocatalysts with seven-membered cyclic diphosphine ligands containing one pendant amine. *J. Am. Chem. Soc.* **135**, 6033–6046 (2013).
33. E. S. Rountree, B. D. McCarthy, T. T. Eisenhart, J. L. Dempsey, Evaluation of homogeneous electrocatalysts by cyclic voltammetry. *Inorg. Chem.* **53**, 9983–10002 (2014).
34. C. Costentin, J.-M. Savéant, Multielectron, multistep molecular catalysis of electrochemical reactions: Benchmarking of homogeneous catalysts. *ChemElectroChem* **1**, 1226–1236 (2014).
35. C. Costentin, S. Drouet, M. Robert, J.-M. Savéant, Turnover numbers, turnover frequencies, and overpotential in molecular catalysis of electrochemical reactions. Cyclic voltammetry and preparative-scale electrolysis. *J. Am. Chem. Soc.* **134**, 11235–11242 (2012).
36. C. Costentin, J.-M. Savéant, Homogeneous molecular catalysis of electrochemical reactions: Manipulating intrinsic and operational factors for catalyst improvement. *J. Am. Chem. Soc.* **140**, 16669–16675 (2018).
37. M. L. Pegis, J. A. S. Roberts, D. J. Wasylenko, E. A. Mader, A. M. Appel, J. M. Mayer, Standard reduction potentials for oxygen and carbon dioxide couples in acetonitrile and *N,N*-dimethylformamide. *Inorg. Chem.* **54**, 11883–11888 (2015).

38. A. Kütt, I. Leito, I. Kaljurand, L. Sooväli, V. M. Vlasov, L. M. Yagupolskii, I. A. Koppel, A comprehensive self-consistent spectrophotometric acidity scale of neutral Brønsted acids in acetonitrile. *J. Org. Chem.* **71**, 2829–2838 (2006).
39. I. M. Kolthoff, M. K. Chantooni, S. Bhowmik, Titration of bases in acetonitrile. *Anal. Chem.* **39**, 1627–1633 (1967).
40. C. T. Carver, B. D. Matson, J. M. Mayer, Electrocatalytic oxygen reduction by iron tetra-arylporphyrins bearing pendant proton relays. *J. Am. Chem. Soc.* **134**, 5444–5447 (2012).
41. S. L. Hooe, C. W. Machan, Dioxygen reduction to hydrogen peroxide by a molecular Mn complex: Mechanistic divergence between homogeneous and heterogeneous reductants. *J. Am. Chem. Soc.* **141**, 4379–4387 (2019).

Acknowledgments: We acknowledge M. L. Pegis for very helpful discussions and F. Menges of the Yale Chemical and Biophysical Instrumentation Center for collecting the HRMS data. **Funding:** We acknowledge support from the NSF grant 1828190 for support of mass spectrometry facilities. This research was supported as part of the Center for Molecular Electrocatalysis, an Energy Frontier Research Center funded by the U.S. Department of Energy, Office of Science, Office of Basic Energy Sciences. D.J.M. gratefully recognizes support from an NSF Graduate Research Fellowship. **Author contributions:** D.J.M. and J.M.M. conceived the project, constructed the scientific arguments, and wrote the paper. B.Q.M. performed x-ray crystallography and solved the structures. D.J.M. performed all other experiments and analyzed and interpreted the data. **Competing interests:** The authors declare that they have no competing interests. **Data and materials availability:** Crystallographic data are available free of charge from the Cambridge Crystallographic Data Centre under reference number 1947226 (**1**). All data needed to evaluate the conclusions in the paper are present in the paper and/or the Supplementary Materials. Additional data related to this paper may be requested from the authors.

Submitted 30 August 2019
Accepted 17 December 2019
Published 13 March 2020
10.1126/sciadv.aaz3318

Citation: D. J. Martin, B. Q. Mercado, J. M. Mayer, Combining scaling relationships overcomes rate versus overpotential trade-offs in O_2 molecular electrocatalysis. *Sci. Adv.* **6**, eaaz3318 (2020).

Science Advances

Combining scaling relationships overcomes rate versus overpotential trade-offs in O_2 molecular electrocatalysis

Daniel J. Martin, Brandon Q. Mercado and James M. Mayer

Sci Adv **6** (11), eaaz3318.
DOI: 10.1126/sciadv.aaz3318

Science Advances (ISSN 2375-2548) is published by the American Association for the Advancement of Science, 1200 New York Avenue NW, Washington, DC 20005. The title *Science Advances* is a registered trademark of AAAS.